Environ. Sci. Technol. **1998**, *32*, 63−70

Advanced Oxidation of Bromide-Containing Waters: Bromate Formation Mechanisms

URS VON GUNTEN* AND YVONNE OLIVERAS

Swiss Federal Institute for Environmental Science and Technology, EAWAG, 8600 Dübendorf, Switzerland

Bromate formation in ozone-based advanced oxidation processes (AOPs) was investigated by laboratory experiments in combination with kinetic modeling. Oxidant concentrations were monitored during the experiments, which allows us to account for the relative contributions of ozone and OH radical pathways. It has been shown by γ-irradiation of bromide-containing solutions in the pH range 6−8 that bromate can be formed by a pure OH radical mechanism and that hypobromous acid/hypobromite (HOBr/OBr^-) is a requisite intermediate in bromate formation. The presence of hydrogen peroxide (H_2O_2), as in H_2O_2-based AOPs, leads to a reduction of HOBr/OBr^- and therefore becomes a key reaction for the control of bromate formation. The steady-state concentration of OH radicals in AOPs is usually not high enough to compensate for this reduction reaction. Therefore, in γ-irradiation experiments, no bromate was formed in the presence of H_2O_2 because OH radicals were the only possible oxidants to further oxidize HOBr/OBr^-. However, in ozone-based AOPs at pH 7, where ozone is present in combination with H_2O_2, bromate was still formed. This was attributed to the oxidation of $Br^•$ by O_3, which was investigated at pH 7. Our experimental findings could be best explained by a corresponding second-order rate constant $k = 1.5 \times 10^8$ M^{-1} s^{-1}.

Introduction

Bromate formation during oxidative treatment of bromide-containing drinking water has been of great concern ever since bromate was classified as potentially carcinogenic by the IARC (International Agency for the Research on Cancer) in 1990 (*1*). In both the United States and the European Community, maximum contaminant levels of 10 μg/L have been set (*2*, *3*). It has been found that these regulations can only be fulfilled in standard ozonation if the processes are carefully optimized (*4*−*6*). For the application of advanced oxidation processes (AOP) such as the combination of O_3 and H_2O_2, the extent of bromate formation is still controversial (*7*−*11*). Some of the studies show that there is more bromate formed in the AOP with respect to conventional ozonation, whereas other investigations find smaller quantities of bromate formed if H_2O_2 is combined with O_3. These differences are largely due to different modes of AOP application. It has been shown that AOPs when compared with a conventional ozonation process lead to higher bromate concentrations, if for both processes the same ozone residual is maintained (*6*). Lower bromate formations result if the amount of dosed ozone is kept constant while increasing the addition of hydrogen peroxide. The findings in full-scale experiments could be explained semi-quantitatively by this classification of the processes. However, it was impossible to quantitate bromate formation on a mechanistic level by only applying the earlier proposed mechanisms that include direct reactions with molecular ozone and reactions with secondary oxidants such OH radicals ($OH^•$) and carbonate radicals (*12*−*14*).

The objective of the present study was to delineate O_3 and $OH^•$ reaction pathways by performing experiments either in combined O_3/H_2O_2 systems or with γ-irradiation where only OH radicals are present as oxidants.

Experimental Section

All experiments were performed in deionized, redistilled water. The pH was buffered with 2 mM phosphate. Titrisol buffers (Merck) were used to calibrate the pH electrode. Hydrogen peroxide-containing solutions were prepared from approximately 30% stock solutions (Perhydrol, Merck, p.a.). No carbonate was added to scavenge OH radicals; the scavenging contribution of carbonate from the atmosphere is only in the order of 1%.

Approach. *(1) Ozonation Experiments.* To compare the experiments with computer-based kinetic simulations, the oxidant concentrations (ozone and OH radicals) and hydrogen peroxide were measured during the experiments. Like this, the overall oxidant concentrations were experimentally fixed and could not be used as fitting parameters. Whereas the concentration of O_3 could be measured directly by its UV absorbance, transient OH radical steady-state concentrations had to be determined indirectly by the decrease of a probe compound, which reacts negligibly with molecular ozone, and thus its disappearance is due to reaction with $OH^•$. Atrazine was chosen for this purpose ($k_{OH,atr} = 3.3 \times 10^9$ M^{-1} s^{-1}; *15*) because of its ease of measurement and its relevance as a micropollutant in drinking water (*6*). Bromide was used as the main OH radical scavenger (to control the lifetime of $OH^•$). The OH radical scavenging by hydrogen peroxide was always in the order of <3%.

(2) γ-Irradiation Experiments. The same concept was applied as in ozonation experiments. To calculate the steady-state concentration of OH radicals *p*-chlorobenzoic acid (PCBA) was used as probe compound ($k_{OH,PCBA} = 6 \times 10^9$ M^{-1} s^{-1}; *15*).

Ozonation and γ-Irradiation. All ozonation experiments were performed directly in a 5-cm quartz cuvette (thermostated at 20 °C) by adding concentrated stock solutions of ozone to the bromide-containing solution with a syringe (*12*, *17*). Hydrogen peroxide was added before the addition of ozone. The initial conditions of the ozonation experiments were $[Br^-]_0 = 0.1-1$ mM, $[O_3]_0 = 40$ μM, $[H_2O_2]_0 = 0.02-0.5$ mM, $[\text{atrazine}]_0 = 0.5$ μM, pH = 7.

All γ-irradiation experiments were performed in a ^{60}Co γ-radiation source with lead shielding (type GAMMACELL, Atomic Energy of Canada; dose rate for water = 2.1 kGy h^{-1} ± 20% in the center of source with lead shielding). The initial conditions of the γ-irradiation experiments were $[Br^-]_0 = 0.05-2$ mM, $[H_2O_2]_0 = 0.01-0.05$ mM, $[PCBA]_0 = 0.5$ μM, pH = 6−8, room temperature. The ionizing radiation resulted in the radiolysis of water to produce H_2O_2, $OH^•$, $H^•$, and e^-_{aq}. All experiments were performed in N_2O-saturated solutions with a N_2O concentration of approximately 0.026 M ($O_2 < 3 \times 10^{-6}$ M). N_2O was added to transform $H^•$ and e^-_{aq} into OH radicals as shown in Table 1. The rate constants for the reactions of $H^•$ and e^-_{aq} with other selected solutes and the

* Author for correspondence: telephone: +41-1-823-5270; fax: +41-1-823-5028; e-mail: vongunten@eawag.ch.

S0013-936X(97)00477-X CCC: $14.00
Published on Web 01/01/1998

TABLE 1. Relevant Reactions of e^-_{aq} and H•

no.	reaction	rate constant (M^{-1} s^{-1})	max concn (M)	k' (s^{-1})	source
1	$e^-_{aq} + N_2O \xrightarrow{H^+} N_2 + {}^\bullet OH$	9.1×10^9	N_2O/0.026	2.4×10^8	18
2	$e^-_{aq} + O_2 \rightarrow O_2^-$	1.9×10^{10}	$O_2/5 \times 10^{-5}$	9.5×10^5	18
3	$e^-_{aq} + OBr^- \xrightarrow{H^+} Br^- + {}^\bullet OH$	2.3×10^{10}	HOBr/5×10^{-5}	1.2×10^6	19
4	$e^-_{aq} + BrO_3^- \xrightarrow{H_2O} BrO_2 + O_2^-$	4×10^9	$BrO_3^-/5 \times 10^{-5}$	2×10^5	19
5	$H^\bullet + N_2O \rightarrow N_2 + {}^\bullet OH$	2.1×10^6	N_2O/0.026	5.5×10^4	20
6	$H^\bullet + O_2 \rightarrow HO_2$	2.1×10^{10}	$O_2/5 \times 10^{-5}$	1.1×10^6	18
7	$H^\bullet + H_2O_2 \rightarrow H_2O + {}^\bullet OH$	$5 \times 10^7/9 \times 10^7$	$H_2O_2/5 \times 10^{-5}$	$2.5-5 \times 10^3$	21/22

calculated first-order rate constants, k', for the competitive consumption of H• and e^-_{aq} are also given in this table. This estimate shows clearly that the main pathway of reactions of H• and e^-_{aq} is controlled by N_2O at the beginning of the irradiation. However, in the course of the irradiation of solutions containing bromide and hydrogen peroxide, the produced oxygen becomes the dominant scavenger of H•. Only a fraction of 4% of H• reacts with H_2O_2. Even at long irradiation times, only about 0.4% of the e^-_{aq} would react with oxygen, 0.5% with OBr^-, and 0.1% with bromate if we assume the maximum measured concentrations of these reactants. The direct radiolysis of the solutes is negligible.

Radical production rates were calculated from the rate of accumulation of H_2O_2 in irradiated air-saturated solutions containing 1 mM and 5 mM sodium formate (pH 6.5). Under these conditions OH•, H•, and e^-_{aq} yield stoichiometric amounts of O_2^-, which disproportionates to H_2O_2. Accounting for the stoichiometric factor ($2\,O_2^- \rightarrow 1H_2O_2$), the resulting total H_2O_2 flux ($f(H_2O_2)_{tot}$) is composed of $1/2f(OH^\bullet) + 1/2f(H^\bullet) + 1/2f(e^-_{aq}) + f(H_2O_2)$ and was 0.17 μM/s with G values ($H^\bullet = 0.65$; $e^-_{aq} = 2.65$; $OH^\bullet = 2.75$; $H_2O_2 = 0.7$) according to ref 23, which stand for the relative proportion of the primary radiolytic formation. The total OH radical flux for N_2O-saturated solutions corresponds to the sum of the fluxes of OH radicals (0.13 μM/s), electrons (0.12 μM/s), and H atoms (0.03 μM/s) and could be calculated to be 0.28 μM/s. The flux of H_2O_2 through direct formation of H_2O_2 in the spur was 0.032 μM/s.

Analysis. Ozone was directly measured by its UV absorbance at 258 nm with a molar extinction coefficient $\epsilon = 3200\ M^{-1}cm^{-1}$ (*15*). Hydrogen peroxide concentrations were determined by the peroxidase−DPD method (*16*). Hypobromous acid was determined by a DPD method using iodine as an intermediate oxidant. Atrazine was determined by HPLC (Hypersil ODS, 5 μm column (Florio)) with an eluent containing 50% H_2O, 25% methanol, and 25% acetonitrile and detected by its UV absorbance at 221 nm. *p*-Chlorobenzoic acid was determined by HPLC (column: Merck Lichrospher 100−105 μm) with an eluent containing 45% 10 mM H_3PO_4 and 55% methanol and detected at 234 nm. The initial concentrations of atrazine and PCBA were 0.5 μM, and their decrease could be measured down to the detection limit of 0.025 μM. Bromate was determined by ion chromatography with conductivity after suppression. An AG9-SC guard and an AS9-SC analytical column (Dionex) were used for the separation. The detection limit was 2 μg/L with a 500-μL loop (*6*). For the chromatographic methods, calibration curves were measured before and after a series of 30−50 samples. Every fifth sample injected was a control standard.

Computer Simulations. Computer simulations of reaction kinetics were performed using the program ACUCHEM, which allows someone to simultaneously solve complicated reaction systems (*24*).

To simulate the ozone decrease, there are two possible approaches: (i) using a complete set of elementary reactions to do an a priori calculation of the ozone depletion and (ii) approach the ozone curves by an empirical model. Even though the ozonation curves could be approached reasonably well by an a priori model, the observed decrease in atrazine representing the simulation of the OH radical concentration could not be predicted. Therefore, the second approach was chosen where a first-order rate constant for ozone was introduced for each experiment to yield a good overlap of experiment and model calculation. The decrease of atrazine was then optimized by the net yield of OH radicals per decomposed ozone. Best results were obtained by an OH radical net yield of 25%, which includes the OH radical yield from ozone decomposition and all the OH• scavenging not accounted for by the a priori kinetic model. This net yield seems relatively low but under the experimental conditions in this study ozone acts as an important OH radical scavenger.

Results and Discussion

Bromate Formation by OH Radicals: Role of H_2O_2. So far, there has been no experimental evidence in the literature for bromate formation by oxidation of Br^- by OH radicals only. In the following we use γ-radiolysis to investigate the OH• mechanism separately from any O_3 involvement. Figure 1 shows bromate formation and hydrogen peroxide decrease in bromide-containing solutions (50 μM) at pH 6 (a), pH 7 (b), and pH 8 (c) for γ-irradiation experiments. For both concentrations of hydrogen peroxide (triangles 50 μM, squares 10 μM) and all three pH values, it decreases linearly with irradiation (OH radical scavenging of $H_2O_2 < 3\%$). The comparison of two different H_2O_2 concentrations at a single pH shows that bromate formation (corresponding open symbols) only starts as soon as hydrogen peroxide approaches zero. The same behavior of H_2O_2 and bromate can be observed over the pH range 6−8, which shows that the system is not limited by pH-dependent reactions.

These experimental findings can be interpreted by the radical reaction sequence for bromate formation in Table 2, which has in part been postulated before (*12*−*14*). For acid−base and hydration equilibria, diffusion-controlled reaction kinetics are assumed. The postulated reaction sequence in Table 2 shows that hypobromous acid (HOBr)/hypobromite (OBr^-) is a requisite intermediate in bromate formation, i.e., there is no bromate formation through the radical pathway without a previous oxidation of bromide to HOBr/OBr^-. In addition to the oxidation processes, HOBr/OBr^- is rapidly reduced by hydrogen peroxide (eq 35) to bromide (*36*) with a second-order rate constant that has been determined recently (*37*). Our experiments show that the rate of the HOBr-HO_2^- reaction is high enough in the pH range 6−8 for complete reduction of HOBr, thus hindering bromate formation in γ-irradiation experiments as long as hydrogen peroxide is in solution. In the pH range of drinking water,

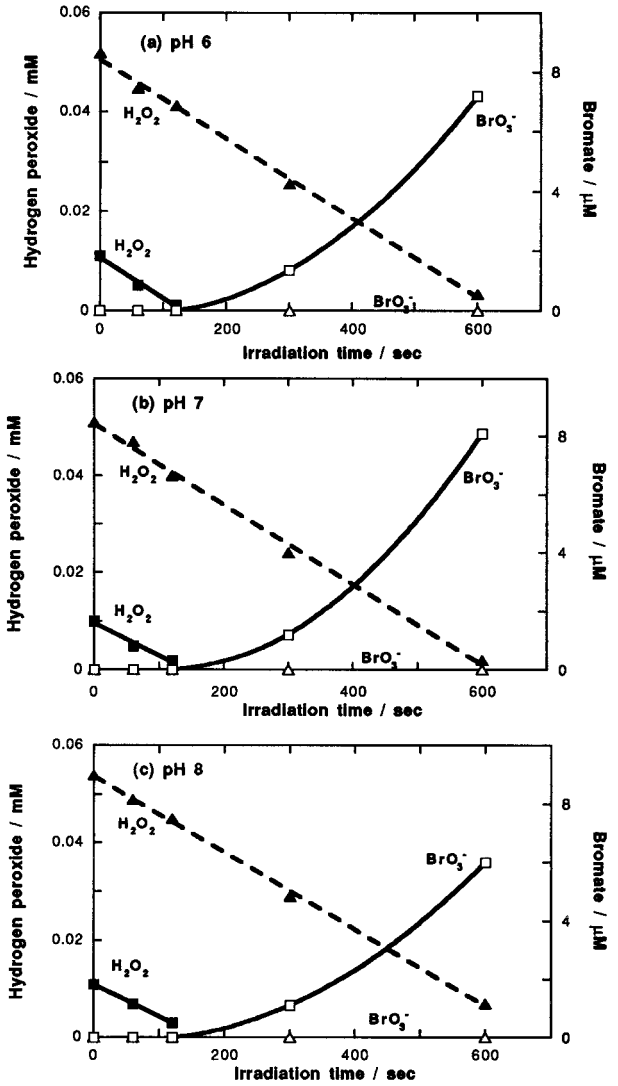

FIGURE 1. γ-Radiolysis: Bromate formation (open symbols) and decrease of hydrogen peroxide (closed symbols) as a function of the irradiation time (dose rate 0.583 Gy/s) at pH 6 (a), pH 7 (b); and pH 8 (c) for two hydrogen peroxide concentrations (closed triangles 50 μM, closed squares 10 μM). Initial conditions: $[Br^-] = 0.05$ mM, 2 mM phosphate, N_2O-saturated solutions.

the two species H_2O_2 and HOBr react very slowly with a rate constant $\ll 10^3$ M^{-1} s^{-1}. This reaction can therefore be neglected. Our findings allow the conclusion that bromate can indeed be formed through a pure OH radical mechanism and that HOBr is a requisite intermediate.

To get a quantitative interpretation of the γ-irradiation results, a series of experiments was performed with high initial bromide concentrations (2 mM) to assure complete scavenging of OH radicals via a known reaction pathway. Figure 2 shows experimental results (symbols) and kinetic simulations (lines, calculated by ACUCHEM) for the species H_2O_2, HOBr, BrO_3^-, and $^\bullet$OH. Again, hydrogen peroxide decreases linearly with the irradiation time (dose), and as soon as it is completely depleted, HOBr starts to build up, followed by bromate formation.

Knowing the fluxes of reactive species, some species shown in Figure 2 can be quantitatively interpreted. Such calculations are performed for the concentration of OH radicals, H_2O_2, and HOBr, and compared with direct measurements.

(1) Steady-State Concentration of OH Radicals. The steady-state concentration of OH radicals for the experiments shown in Figure 2 can either be measured directly by the decrease of a probe compound (PCBA), or it can be calculated by the difference in the rate of formation of OH radicals ($f(OH^\bullet)$) and the rate of its scavenging by bromide:

$$\frac{d[OH^\bullet]}{dt} = f(OH^\bullet) - k''[OH^\bullet]_{ss}[Br^-] = 0 \qquad (36)$$

$$[OH^\bullet]_{ss} = \frac{f(OH^\bullet)}{k''[Br^-]} = \frac{0.28 \times 10^{-6}\ M\ s^{-1}}{(1.2 \times 10^9\ M^{-1}\ s^{-1}) \times (2 \times 10^{-3}\ M)} = 1.2 \times 10^{-13}\ M \qquad (37)$$

$f(OH^\bullet)$ in M s^{-1} is the flux of $OH^\bullet$ into the system, determined experimentally (see above); k'' is the apparent rate constant for reaction of $OH^\bullet$ with Br-, including reactions 8−10; and $k'' = 1.2 \times 10^9$ M^{-1} s^{-1}, for derivation see ref 38. A steady-state concentration of OH radicals of $(1.06 \pm 0.1) \times 10^{-13}$ M was determined from the decrease of PCBA under the same experimental conditions. The calculated and experimentally determined $[OH^\bullet]_{ss}$ are not significantly different and confirm the experimental intention to use bromide as the major scavenger of OH radicals in this system.

(2) Hydrogen Peroxide. The consumption of dosed H_2O_2 is controlled by its reaction with HOBr (eq 35). From reactions 8−16 in Table 2, it can be seen that stoichiometrically two OH radicals are required to produce one HOBr molecule. Therefore, the change in the H_2O_2 concentration can be formulated as the difference between H_2O_2 dosed, the rate of H_2O_2 formation, and the production of HOBr:

$$[H_2O_2](t) = [H_2O_2]_0 + f(H_2O_2)t - \frac{1}{2}\{f(OH^\bullet) + f(H^\bullet) + f(e^-_{aq})\}t \qquad (38)$$

where f signifies flux and t is the irradiation time.

The irradiation time for which the H_2O_2 is depleted can be calculated if the initial dosage of H_2O_2 ($[H_2O_2]_0$) is known and the additional radiolytical production is taken from the G values and the calibration above. The theoretical irradiation time calculated (by eq 38) for the complete depletion of 21 μM dosed hydrogen peroxide is 196 s (114 Gy). This time span matches perfectly with the experimental finding of 195 s (113.7 Gy) shown in Figure 2. This stoichiometric check based on the H_2O_2-HOBr reaction is another confirmation of the proposed mechanism involving HOBr as a requisite reaction intermediate.

(3) HOBr and BrO_3^-. Figure 2 also shows the evolution of hypobromous acid and bromate. A buildup of HOBr was only observed after H_2O_2 had approached zero. The buildup of HOBr is controlled by its formation through reactions 8−16 and its reduction through reactions 34 and 35. Superoxide radicals are formed through reaction of $H^\bullet$ with oxygen, which is produced from the reduction of HOBr with H_2O_2 (eq (35). According to Table 1, all $H^\bullet$ reacts with oxygen at this stage of the reaction ($[O_2] \geq 2 \times 10^{-5}$ M, $t \geq 200$ s). Hence, the initial rate of HOBr formation can be formulated resulting from oxidizing (OH radicals and electrons) and reducing (H atoms and hydrogen peroxide) processes:

$$\frac{d[HOBr]}{dt} = \frac{1}{2}\{f(OH^\bullet) + f(e^-_{aq})\} - f(H^\bullet) - f(H_2O_2) = 6.5 \times 10^{-8}\ M\ s^{-1} \qquad (39)$$

This calculated initial rate matches well with the rate derived from the initial slope of the HOBr curve in Figure 2, which is 6.7×10^{-8} M s^{-1}. After the initial linear increase of HOBr,

TABLE 2. Reactions Occurring during γ-Irradiation of Bromide- and Hydrogen Peroxide-Containing Solutions[a]

no.	reaction	k_+, k_-, or K	source
8	$Br^- + {}^\bullet OH \rightleftarrows BrOH^-$	$10^{10}\ M^{-1}\ s^{-1}$, $3.3 \times 10^7\ s^{-1}$	25
9	$BrOH^- \rightarrow Br^\bullet + OH^-$	$4 \times 10^6\ s^{-1}$	25
10	$Br^\bullet + OH^- \rightarrow BrOH^-$	$1.3 \times 10^{10}\ M^{-1}\ s^{-1}$	26
11	$BrOH^- + H^+ \rightarrow Br^\bullet + H_2O$	$4.4 \times 10^{10}\ M^{-1}\ s^{-1}$	27
12	$BrOH^- + Br^- \rightarrow Br_2^- + OH^-$	$2 \times 10^8\ M^{-1}\ s^{-1}$	27
13	$Br^\bullet + Br^- \rightleftarrows Br_2^-$	$10^{10}\ M^{-1}\ s^{-1}$, $10^5\ s^{-1}$	25
14	$Br_2^- + Br_2^- \rightarrow Br_3^- + Br^-$	$2 \times 10^9\ M^{-1}\ s^{-1}$	28
15	$Br_3^- \rightleftarrows Br_2 + Br^-$	$8.3 \times 10^8\ s^{-1}$, $10^{10}\ M^{-1}\ s^{-1}$	29
16	$Br_2 + H_2O \rightleftarrows HOBr + H^+ + Br^-$	$5.8 \times 10^{-9}\ M^2$	29
17	$HOBr \rightleftarrows OBr^\bullet + H^+$	1.58×10^{-9} M	30
(18	$Br_2^- + OBr^- \rightarrow BrO^\bullet + 2Br^-$)	$8 \times 10^7\ M^{-1}\ s^{-1}$?	18
19	$Br^\bullet + OBr^- \rightarrow BrO^\bullet + Br^-$	$4 \times 10^9\ M^{-1}\ s^{-1}$	26
20	${}^\bullet OH + OBr^- \rightarrow BrO^\bullet + OH^-$	$4.5 \times 10^9\ M^{-1}\ s^{-1}$	18
21	${}^\bullet OH + HOBr \rightarrow BrO^\bullet + H_2O$	$2 \times 10^9\ M^{-1}\ s^{-1}$	18
22	$2BrO^\bullet + H_2O \rightarrow OBr^- + BrO_2^- + 2H^+$	$5 \times 10^9\ M^{-1}\ s^{-1}$	18
23	$BrO^\bullet + BrO_2^- \rightarrow OBr^- + BrO_2$	$3.4 \times 10^8\ M^{-1}\ s^{-1}$	18
24	$Br_2^- + BrO_2^- \rightarrow OBr^- + BrO^\bullet + Br^-$	$8 \times 10^7\ M^{-1}\ s^{-1}$	18
25	${}^\bullet OH + BrO_2^- \rightarrow BrO_2 + OH^-$	$1.9 \times 10^9\ M^{-1}\ s^{-1}$	18
26	${}^\bullet OH + BrO_2 \rightarrow BrO_3^- + H^+$	$2 \times 10^9\ M^{-1}\ s^{-1}$	31
27	$BrO_2 + BrO_2 \rightleftarrows Br_2O_4$	$1.4 \times 10^9\ M^{-1}\ s^{-1}$, $7 \times 10^7\ s^{-1}$	18
28	$Br_2O_4 + OH^- \rightarrow BrO_3^- + BrO_2^- + H^+$	$7 \times 10^8\ s^{-1}$	18
29	$H_2O_2 + {}^\bullet OH \rightarrow HO_2 + H_2O$	$2.7 \times 10^7\ M^{-1}\ s^{-1}$	18
30	$HO_2^- + {}^\bullet OH \rightarrow O_2^- + H_2O$	$7.5 \times 10^9\ M^{-1}\ s^{-1}$	32
31	$H_2O_2 \rightleftarrows HO_2^- + H^+$	2.5×10^{-12} M	33
32	$HO_2 \rightleftarrows O_2^- + H^+$	1.6×10^{-5} M	34
33	${}^\bullet OH + {}^\bullet OH \rightarrow H_2O_2$	$5.5 \times 10^9\ M^{-1}\ s^{-1}$	32
34	$O_2^- + HOBr \rightarrow O_2 + Br^\bullet + OH^-$	$3.5 \times 10^9\ M^{-1}\ s^{-1}$	35
35	$HO_2^- + HOBr \rightarrow Br^- + O_2 + H_2O$	$7.6 \times 10^8\ M^{-1}\ s^{-1}$	37

[a] k_+, forward reaction; k_-, backward reaction; K, equilibrium constant.

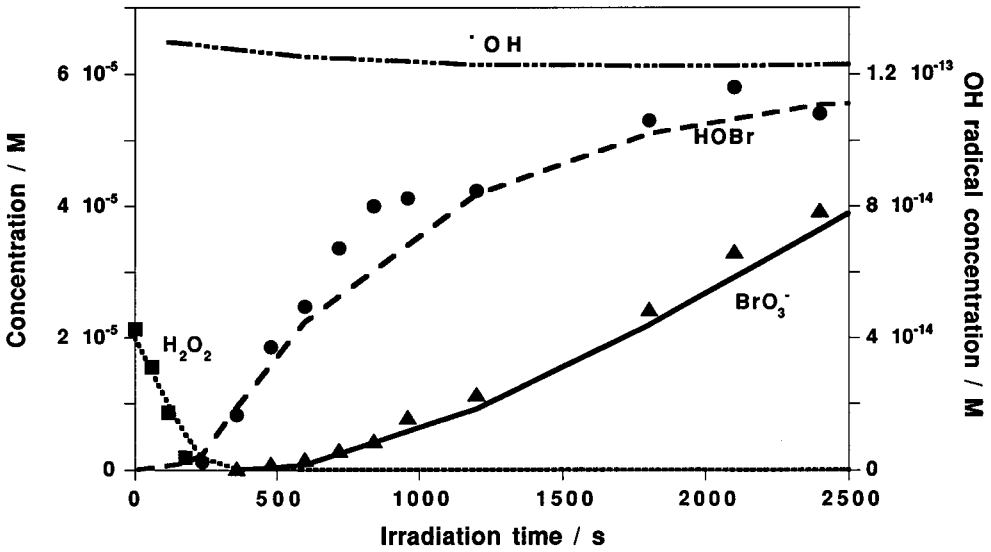

FIGURE 2. γ-Radiolysis: Hypobromous acid, bromate formation, decrease of hydrogen peroxide, and calculated OH radical concentration as a function of the irradiation time (dose rate 0.583 Gy/s) at pH 7 for N_2O-saturated solutions. Symbols represent experimental data, and curves represent the kinetic simulations. Initial conditions: $[Br^-] = 2$ mM, $[H_2O_2] = 0.021$ mM, 2 mM phosphate.

it reaches a steady-state concentration of approximately 55 μM, which cannot be explained by a simple approximation.

The concentrations of hydrogen peroxide, hypobromous acid, and bromate shown in Figure 2 were calculated by kinetic simulations including the radical fluxes and the equations given in Table 2. Kinetic modeling (lines) of all species showed good agreement with the measured data (symbols). Model calculations yield an OH radical steady-state concentration of 1.2×10^{-13} M (Figure 2, top curve), which is also within the experimental error of the data shown above (1.2×10^{-13} M based on flux calculations, 1.06×10^{-13} M based on the decrease of PCBA). Some deviations between experiments and kinetic calculations may result from the experimental variations due to positioning of the sample in the ^{60}Co source.

Bromate formation has a lag-phase with respect to HOBr formation. This is plausible since bromate has HOBr as a requisite intermediate and a measurable buildup of bromate can only start when the concentration of hypobromous acid reaches a certain level. The comparison of the experimental data with model calculations show again an almost perfect agreement (Figure 2). It could be shown by kinetic modeling that bromate is formed predominantly by the reaction sequence 22, 25, 27, and 28 and only to a fraction of 10% by the sequence 22, 25, and 26.

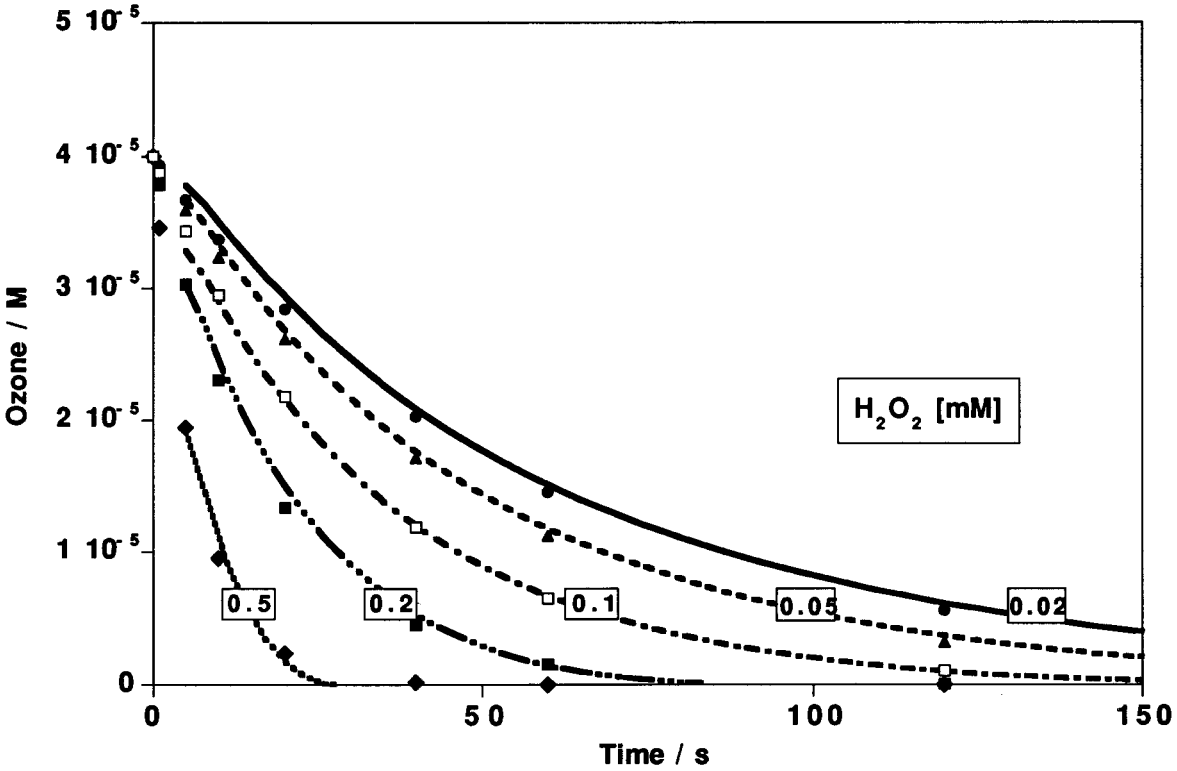

FIGURE 3. Combined O_3/H_2O_2 experiments for varying $[H_2O_2]_0$ concentrations: Decrease of the concentration of ozone as a function of the reaction time at pH 7. Curves, experimental data; symbols, kinetic simulations. $[O_3]_0 = 4 \times 10^{-5}$ M (2 mg/L), $[Br^-]_0 = 0.1$ mM, $[H_2O_2]_0$ varying as indicated on the curves.

TABLE 3. Molecular Ozone Reactions for Bromate Formation

no.	reaction	rate constant (M^{-1} s^{-1})	source
40	$Br^- + O_3 \rightarrow OBr^- + O_2$	160	30
41	$OBr^- + O_3 \rightarrow Br^- + O_2$	330	30
42	$OBr^- + O_3 \rightarrow BrO_2^- + O_2$	100	30
43	$BrO_2^- + O_3 \rightarrow BrO_3^- + O_2$	$\gg 1 \times 10^5$[a]	30

[a] Bromate formation is not sensitive to rate of this reaction; 1×10^5 M^{-1} s^{-1} was assumed for kinetic modeling.

In the kinetic simulations, a good agreement could only be achieved when neglecting reaction 18. If this reaction is included, the concentration of HOBr is underestimated approximately a factor of 4, and bromate is overpredicted by a factor of 2 when compared with measured values. The rate constant for reaction 18 was measured from pulse-radiolysis experiments of bromide-containing solutions at pH 12 by following the decrease of Br_2^- in presence of OBr^- (*18*). However, in the original work the authors did not evaluate the postulated reaction carefully enough and just proposed one possibility. From our results it appears that reaction (18) is not occuring as it was proposed by ref 18. Therefore, we do not include the reaction in our kinetic simulation model.

Bromate Formation in an Advanced Oxidation Process (O_3/H_2O_2). If a combination of ozone and hydrogen peroxide is applied, both the reactions shown in Table 2 and the additional reactions involving molecular ozone (Table 3) are important for bromate formation. This combined mechanism also leads to $HOBr/OBr^-$ as a requisite intermediate that is subject to rapid reduction to Br^- by H_2O_2 (*37*). For an ozone concentration of 2 mg/L (50 μM), the first-order rate constant for the oxidation of $HOBr/OBr^-$ by ozone is 4×10^{-5} s^{-1}. For a typically applied w/w ratio of O_3/H_2O_2 of 3, the first-order rate constant for $HOBr/OBr^-$ reduction by H_2O_2 (20 μM) is 0.38 s^{-1} at pH 7. This estimate of the competition kinetics shows that in combined processes O_3/H_2O_2 undetectable amounts of bromate should be produced for the range of bromide concentrations typically found in water treatment. However, under such treatment conditions in full-scale experiments, high bromate concentrations can still be formed (*6*). To further clarify this paradox between experimental findings and model predictions, we performed experiments with varying hydrogen peroxide and bromide concentrations.

(1) Influence of Hydrogen Peroxide. Ozone depletion curves for varying H_2O_2 (0.02−0.5 mM) and constant bromide concentrations (0.1 mM) are shown in Figure 3 for a pH of 7. The corresponding results for atrazine and H_2O_2 are shown in Figure 4a; bromate formation after complete depletion of ozone is depicted in Figure 4b. The measured ozone depletion as shown in Figure 3 (lines) gets faster with increasing H_2O_2 concentration. This can be well modeled (symbols) by the combination of the reactions shown in Tables 2 and 3 and an additional empirical first-order reaction for ozone depletion.

As shown in Figure 4a, the maximum decrease of atrazine is reached at an initial H_2O_2 concentration of about 0.3 mM; further increases in H_2O_2 concentration do not lead to significantly better removal. The model reflects this behavior quite well, within the experimental error of the rate constant $k_{OH,atr}$. This means that the assumed net OH radical yield, and therefore the exposure to OH radicals ($\int[OH^\bullet]dt$), is well reflected by the model. The final H_2O_2 concentrations as a function of the initial H_2O_2 concentrations are also shown in Figure 4a. In general, the H_2O_2 concentration decreases by about 75% of the added ozone concentration due to the reaction between H_2O_2 and formed $HOBr/OBr^-$ (i.e., reaction 35). The agreement between experiments (symbols) and kinetic modeling (line) is reasonable considering the simplifications in the model (no direct reaction of HO_2^- and O_3 included in the model). Therefore, measured and modeled ozone and atrazine concentrations allow the assumption that

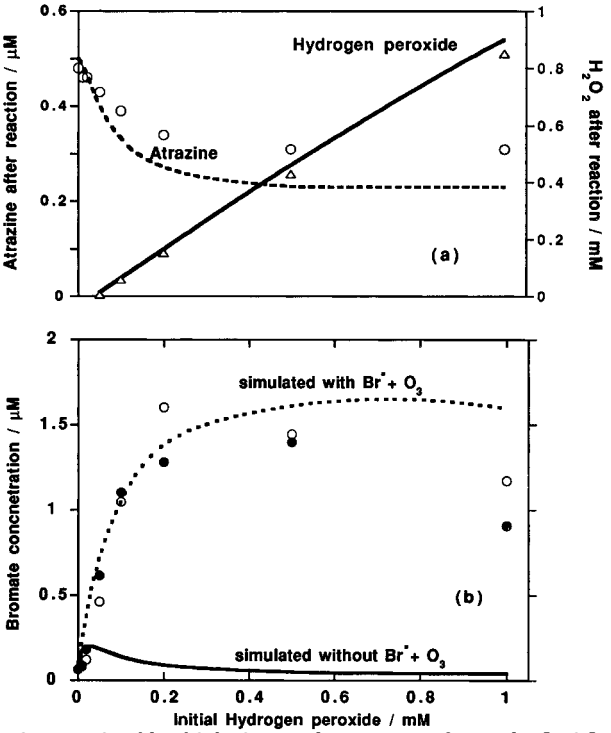

FIGURE 4. Combined O_3/H_2O_2 experiments at pH 7 for varying $[H_2O_2]_0$: Symbols represent experimental data; curves represent the kinetic simulations. (a) Final concentrations of atrazine (circles) and hydrogen peroxide (triangles) as a function of the hydrogen peroxide dose. (b) Bromate concentrations after depletion of ozone for duplicate experiments. Two kinetic simulations are shown including or excluding the reaction between Br• and O_3. $[O_3]_0 = 4 \times 10^{-5}$ M (2 mg/L), $[Br^-]_0 = 0.1$ mM, [atrazine]$_0 = 0.5$ µM, $[H_2O_2]_0$ varying as indicated.

we know the overall oxidant concentration in our experiments. This knowledge enables us to model bromate formation under controlled conditions.

In Figure 4b, bromate formation is shown for duplicate experiments (open and closed circles). With an increasing hydrogen peroxide concentration, we observe an increase in bromate that eventually decreases slowly again. Modeling of the data by the combination of the reactions shown in Tables 2 and 3 yields bromate as shown by the solid line in the lower part of Figure 4b. For small H_2O_2 concentrations ($\leq$0.02 mM), the experiments are well represented by the model. However, when the H_2O_2 concentration is increased, the model completely underestimates the experimental findings. Since we have shown in our γ-irradiation experiments that in the presence of H_2O_2 all HOBr/OBr^- is reduced to Br^-, there has to be a direct mechanism for bromate formation not involving HOBr/OBr^- as a requisite reaction intermediate. However, again from the γ-radiolysis experiments, we know that HOBr/OBr^- is a requisite reaction intermediate if OH radicals are the only oxidants. Therefore, in the presence of molecular ozone a further reaction has to be postulated:

$$O_3 + Br^\bullet \rightarrow BrO^\bullet + O_2 \qquad (44)$$

This reaction (44) is well known from gas phase chemistry where it is reported to be very fast (*39*). By an iterative process, we optimized the rate constant for reaction 44 by including reaction 44 and the reactions in Tables 2 and 3 and obtained the best agreement for the bromate concentration in Figure 4b with a rate constant of $k_{44} = 1.5 \times 10^8$ M^{-1} s^{-1}. The result of model calculations including reaction 44 is shown in Figure 4b by the upper bromate formation curve. The model calculations for bromate now are in good agreement with the experimental data, with some deviations at high H_2O_2 concentrations. Our model does not predict the slight decrease in bromate formation for initial H_2O_2 concentrations above 0.5 mM. The discrepancy might be due to the fact that for high hydrogen peroxide concentrations small differences in the ozone profiles (experiment vs model) are more critical in terms of the overall oxidant budget of the reaction system.

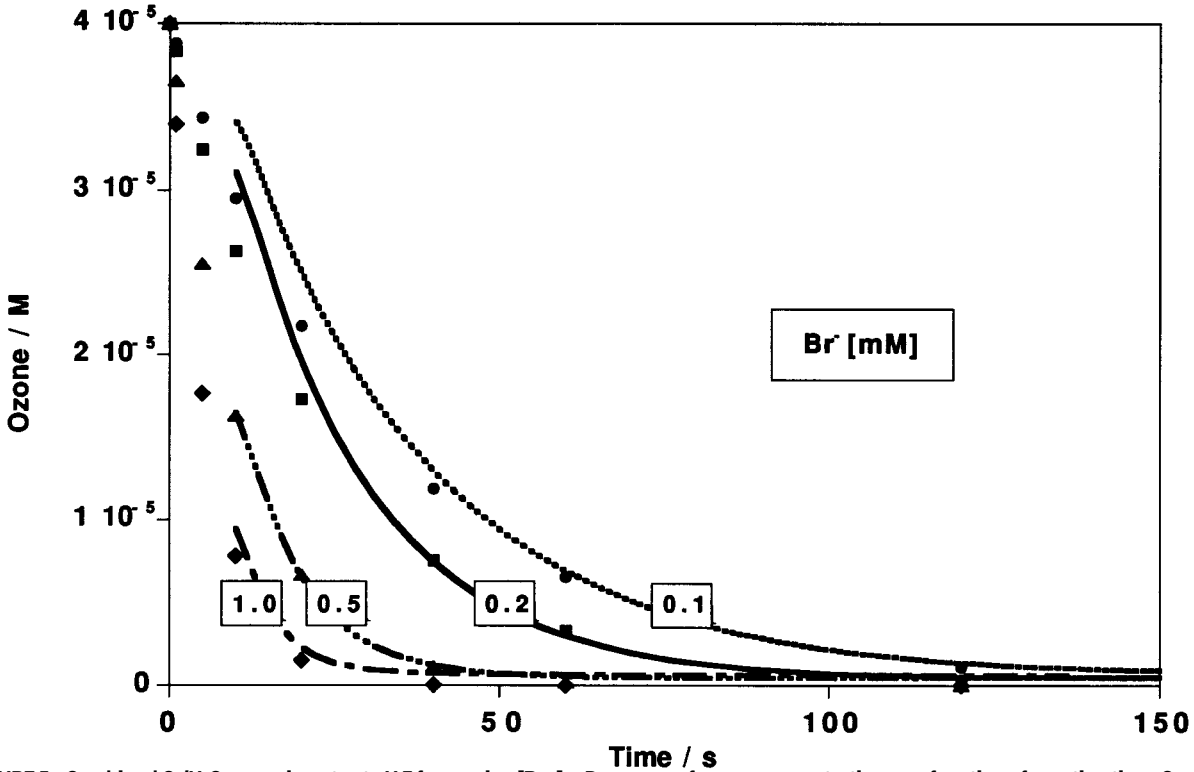

FIGURE 5. Combined O_3/H_2O_2 experiments at pH 7 for varying $[Br^-]_0$: Decrease of ozone concentration as a function of reaction time. Curves, experimental data; symbols, kinetic simulations. $[O_3]_0 = 4 \times 10^{-5}$ M (2 mg/L), $[H_2O_2]_0 = 0.1$ mM, $[Br^-]_0$ varying as indicated on the curves.

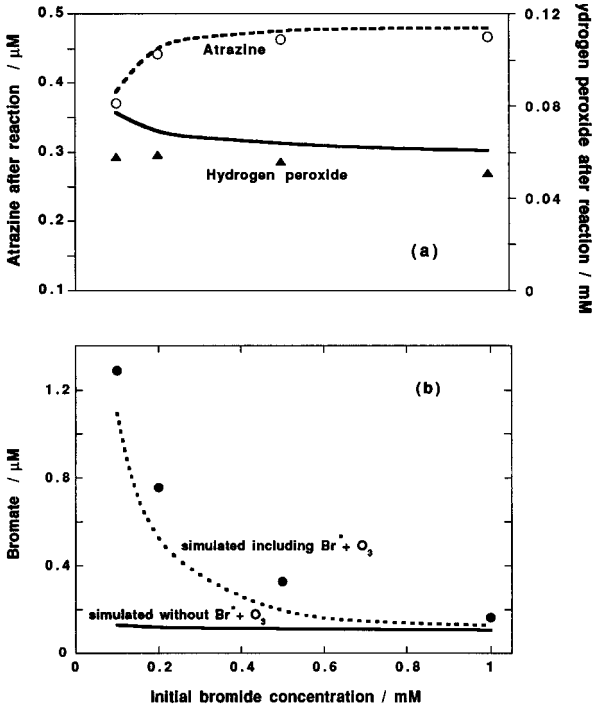

FIGURE 6. Combined O_3/H_2O_2 experiments at pH 7 for varying bromide concentrations: Symbols represent experimental data; curves represent the kinetic simulations. (a) Final concentrations of atrazine (open circles) and hydrogen peroxide (triangles) as a function of the initial bromide concentration. (b) Bromate concentrations (closed circles) after complete depletion of ozone. Two kinetic simulations are shown including or excluding the reaction between Br˙ and O_3. $[O_3]_0 = 4 \times 10^{-5}$ M (2 mg/L), $[H_2O_2]_0 = 0.1$ mM, $[atrazine]_0 = 0.5\ \mu$M, $[Br^-]_0$ varying as indicated.

(2) Influence of Bromide. To further test the mechanism including reaction 44, a series of experiments was performed at pH 7 where the initial H_2O_2 concentration was kept constant at 0.1 mM while the bromide concentration was varied between 0.1 and 1 mM. The ozone depletion curves for these experiments are shown in Figure 5, while the corresponding data for atrazine, H_2O_2, and bromate are presented in Figure 6a,b.

With increasing initial concentrations of bromide, a faster depletion of ozone is observed (Figure 5). This is a result of the direct reaction of ozone with bromide. The model calculations for ozone depletion were obtained using an empirical first-order rate equation as described earlier. There is again good agreement between experimental (lines) and modeled data (symbols). Therefore, the oxidation processes by molecular ozone are well defined for further modeling.

In Figure 6a, the measured concentrations (symbols) of atrazine and hydrogen peroxide for complete depletion of ozone are shown as a function of the initial bromide concentration. For bromide concentrations >0.2 mM, almost no decrease of atrazine has been measured, reflecting very low concentrations of OH radicals. For lower bromide concentrations, an atrazine decrease of up to 30% of the initial concentration of 0.5 μM was observed. The model calculations (line) were obtained as above by fitting an empirical net yield of OH˙ per ozone consumed to the experimental data. The good agreement with the measured atrazine data indicates that the model is reasonably well calibrated with respect to the exposure to OH radicals, i.e., $\int[OH^\bullet]dt$.

In all four experiments shown in Figure 6a, the measured H_2O_2 concentration (symbols) decreases by approximately the equivalent of the ozone added. This is due to the formation of $HOBr/OBr^-$ and its subsequent reduction by H_2O_2. Kinetic calculations (line) predict the same behavior within certain limits (ozone−hydrogen peroxide reactions are not included). Figure 6b shows the corresponding bromate formation data. The measured bromate formation (circles) decreases as the initial bromide concentration increases. This is due to the enhancement of the direct reaction of bromide with ozone-forming $HOBr/OBr^-$, which is rapidly reduced by H_2O_2. As all the O_3 is consumed in the oxidation of Br^- to $HOBr/OBr^-$, there is no residual O_3 to further oxidize Br˙.

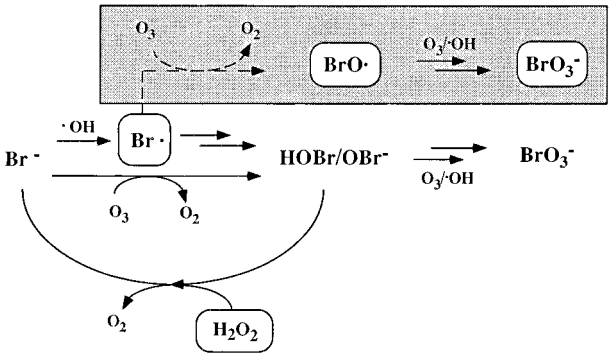

FIGURE 7. Schematic representation of bromate formation in hydrogen peroxide-based advanced oxidation processes.

Model calculations (lines) for the data shown in Figure 6b were again performed using the equations shown in Tables 2 and 3 (solid line) and accounting for reaction 44 (dashed line). The simulation for the reaction system without eq 44 shows that the direct reactions of bromide with ozone cannot account for the measured bromate formation. However, including reaction 44, a decent agreement between experimental data and model calculations can be observed.

In conclusion, a simplified version of the reaction mechanism based on the experimental findings is depicted in Figure 7. The conventional mechanism including oxidation of bromide to $HOBr/OBr^-$ by ozone and/or OH radicals and its further oxidation by ozone and OH radicals is shown in the middle of Figure 7. This mechanism including $HOBr/OBr^-$ as a requisite intermediate is affected by H_2O_2, which forms bromide by a fast reduction process. If both ozone and hydrogen peroxide are present in an AOP, an additional oxidation process has to be included in order to explain the measured bromate formation. It involves the oxidation of the Br radical with O_3 to BrO˙, which is an important precursor for bromate formation (compare to Table 2). From this study, it can also be concluded that the addition of H_2O_2 as a control option to minimize bromate formation does not apply to ozonation processes because the direct reaction of the Br radical with ozone has to be considered. In regard to the different application modes of the O_3/H_2O_2, this reaction might explain the differences in bromate formation that have been reported in the literature.

Acknowledgments

The authors thank J. Hoigné and M. Elovitz for fruitful discussions and reviewing the manuscript.

Literature Cited

(1) *WHO. IARC Monographs on the evaluation of carcinogenic risks to humans, Vol 52*; WHO: Geneva, 1990.
(2) *Fed. Regist.* **1994**, *59* (145), 38668.
(3) Amtsblatt der Europäischen Gemeinschaften. N.. C 131/5, 1995.
(4) Legube, B.; Bourgibot, M. M.; Deguin, A.; Fielding, M.; Kruithof, J. C.; Mallevialle, J.; Matia, L.; Montiel, A.; Wibourn, J. *Proceedings of the 12th Ozone World Congress* Lille, 1995; Instaprint S. A.: Tours, 1995; Vol. 1, pp 129−153.
(5) Lefebre, E.; Racaud, P.; Parpaillon, Th.; Deguin, A. *Ozone Sci. Eng.* **1995**, *17*, 311−327.

(6) von Gunten, U.; Bruchet, A.; Costentin, E. *J. Am. Water Works Assoc.* **1996**, *88* (June), 53−65.
(7) Croué, J. P.; Koudjonou, B. K.; Legube, B. *Ozone Sci. Eng.* **1996**, *18*, 1−18.
(8) Kruithof, J. C.; Meijers, R. T.; Schippers, J. C. *Water Supply* **1993**, *11*, 331−342.
(9) Daniel, P.; Meyerhofer, P. Ozone and bromide ion: treatability issues. *Proceedings of the 11th Ozone World Congress*, San Francisco; Port City Press, Inc.: San Francisco, 1993; Vol. 1, S9, pp 11−27.
(10) Siddiqui, M. S.; Amy, G. L.; Rice, R. G. *J. A. Water Works Assoc.* **1995**, *87* (Oct), 58−70.
(11) Krasner, S. W.; Glaze W. H.; Weinberg, H. S.; Daniel, P. A.; Najm, I. N. *J. Am. Water Works Assoc.* **1993**, *85* (Jan), 73−81.
(12) von Gunten, U.; Hoigné, J. *Environ. Sci. Technol.* **1994**, *28*, 1234−1242.
(13) Yates, R. S.; Stentstrom, M. K. *Proc. AWWA Annual Conf.*, San Antonio, 1993.
(14) Westerhoff, P. Ozone oxidation of bromide and natural organic matter. Ph.D. Dissertation, University of Colorado, Boulder, 1995.
(15) Bader, H.; Hoigné, J. In preparation.
(16) Bader, H.; Sturzenegger, V.; Hoigné, J. *Water Res.* **1988**, *22*, 1109−1115.
(17) Hoigné, J.; Bader, H. *Water Res.* **1981**, *15*, 449−456.
(18) Buxton, G. V.; Greenstock, C. L.; Helman, W. R.; Ross, A. B. *J. Phys. Chem. Ref. Data* **1988**, *17*, 513−886.
(19) Buxton, G. V.; Dainton, F. S. *Proc. R. Soc. London A* **1968**, *304*, 427−439.
(20) Czapski, G.; Peled, E. *Isr. J. Chem.* **1968**, *6*, 421−436.
(21) Elliot, A. *J. Radiat. Phys. Chem.* **1989**, *34*, 753−758.
(22) Sweet, J. P.; Thomas, J. K. *J. Phys. Chem.* **1964**, *68*, 1363−1368.
(23) Sedlak, D. L.; Hoigné, J. *Environ. Sci. Technol.* **1994**, *28*, 1898−1906.
(24) Braun, W.; Herron, J. T.; Kahanar, D. K. *Int. J. Chem. Kinet.* **1988**, *20*, 51−62.
(25) Zehavi, D.; Rabani J. *J. Phys. Chem.* **1972**, *76*, 312−319.
(26) Kläning, U. K.; Wolff, T. *Ber. Bunsen-Ges. Phys. Chem.* **1985**, *89*, 243−245.
(27) Mamou, A.; Rabani, J.; Behar, D. *J. Phys. Chem.* **1977**, *81*, 1447−1448.
(28) Sutton, H. C.; Adams, G. E.; Boag, J. W.; Michael, B. D. In *Pulse Radiolysis*; Ebert, M., Keene, J. P., Swallow, A. J., Baxendale, J. H., Eds.; Academic Press: London, 1965; pp 61−81.
(29) Sidgwick, N. V. *The chemical elements and their compounds, Vol. II*; Oxford Press: Oxford, 1952; p 1219.
(30) Haag, W. R.; Hoigné, J. *Environ. Sci. Technol.* **1983**, *17*, 261−267.
(31) Field, R. J.; Raghavan, N. V.; Brunner, J. G. *J. Phys. Chem.* **1982**, *86*, 2443−2449.
(32) Christensen, H.; Sehested, K.; Corfitzen, H. *J. Phys. Chem.* **1982**, *86*, 1588−1590.
(33) Staehelin, J.; Hoigné, J. *Environ. Sci. Technol.* **1982**, *16*, 667−681.
(34) Bielski, B.; Cabelli, D. E.; Arudi, R. L.; Ross, A. B. *Phys. Chem. Ref. Data* **1988**, *14*, 1041−1100.
(35) Schwarz, H. A.; Bielski, B. H. J. *J. Phys. Chem.* **1986**, *90*, 1445−1448.
(36) Taube, H. *J. Am. Chem. Soc.* **1942**, *64*, 2468−2474.
(37) von Gunten, U.; Oliveras, Y. *Water Res.* **1997**, *31*, 900−906.
(38) von Gunten, U.; Hoigné, J. *Disinfection By-products in Water Treatment*; Minear, R. A., Amy, G. L., Eds.; CRC Press Inc.: Boca Raton, 1996; pp 187−206.
(39) Aktinson, R.; Baulch, D. L.; Cox, R. A.; Hampson, R. F., Jr.; Kerr, J. A.; Troe, J. *Atmos. Environ.* **1992**, *26A*, 1187−1230.

Received for review May 29, 1997. Revised manuscript received September 26, 1997. Accepted October 6, 1997.[⊗]

ES970477J

[⊗] Abstract published in *Advance ACS Abstracts*, November 15, 1997.